



1 **Comparison of key absorption and optical properties between pure**
2 **and transported anthropogenic dust over East and Central Asia**

3 Jianrong Bi¹, Jianping Huang^{1*}, Brent Holben²

4

5 ¹Key Laboratory for Semi-Arid Climate Change of the Ministry of Education, College of
6 Atmospheric Sciences, Lanzhou University, Lanzhou, 730000, China

7 ²NASA Goddard Space Flight Center, Greenbelt, Maryland, USA

8

9 *Submitted to: ACP Special Issue*

10

11

12

13

14

15

16

17

18

19

20

21

22

23

24

25

26

27

28 *Correspondence to: Jianping Huang (hjp@lzu.edu.cn)

29



30 **Abstract.** Asian dust particulate is one of the primary aerosol constituents in the
31 Earth-atmosphere system that exerts profound influences on environmental quality,
32 human health, marine biogeochemical cycle and Earth's climate. To date, the
33 absorptive capacity of dust aerosol generated from Asian desert region is still an open
34 question. In this article, we compile columnar key absorption and optical properties of
35 mineral dust over East and Central Asia areas by utilizing the multi-year quality
36 assured datasets observed at 13 sites of the Aerosol Robotic Network (AERONET).
37 We identify two types of Asian dust according to threshold criteria from previously
38 published literature. (I) The particles with high aerosol optical depth at 440 nm
39 ($\text{AOD}_{440} \geq 0.4$) and low Ångström wavelength exponent at 440-870 nm ($\alpha < 0.2$) are
40 defined as Pure Dust (PDU) that decrease disturbance of other non-dust aerosols and
41 keep high accuracy of pure Asian dust. (II) The particles with $\text{AOD}_{440} \geq 0.4$ and
42 $0.2 < \alpha < 0.6$ are designated as Transported Anthropogenic Dust (TDU), which are
43 mainly dominated by dust aerosol and might mix with other anthropogenic aerosol
44 types. Our results reveal that the primary components of high AOD days are
45 predominant by dust over East and Central Asia regions even if their variations rely
46 on different sources, distance from the source, emission mechanisms, and
47 meteorological characteristics. The overall mean and standard deviation of
48 single-scattering albedo, asymmetry factor, real part and imaginary part of complex
49 refractive index at 550 nm for Asian PDU are 0.935 ± 0.014 , 0.742 ± 0.008 ,
50 1.526 ± 0.029 , 0.00226 ± 0.00056 , respectively, while corresponding values are
51 0.921 ± 0.021 , 0.723 ± 0.009 , 1.521 ± 0.025 , and 0.00364 ± 0.0014 for Asian TDU.
52 Aerosol shortwave direct radiative effects at the top of the atmosphere (TOA), at the
53 surface (SFC), and in the atmospheric layer (ATM) for Asian PDU ($\alpha < 0.2$) and TDU
54 ($0.2 < \alpha < 0.6$) computed in this study, are a factor of 2 smaller than the results of OPAC
55 Mineral accumulated (Mineral acc.) and transported (Mineral tran.) modes. Therefore,
56 we are convinced that our results hold promise of updating and improving accuracies
57 of Asian dust characteristics in present-day remote sensing applications and regional
58 or global climate models.



59 **1. Introduction**

60 Airborne dust particle (also called mineral dust) is recognized as one of the most
61 important aerosol species in the tropospheric atmosphere, which accounts for about
62 30% of the total aerosol loading and extinction aerosol optical depth on a global scale
63 (Perlitz et al., 2001; Kinne et al., 2006; Chin et al., 2009; Huang et al., 2014). High
64 concentrations of dust aerosols hanging over desert source regions and invasive
65 downstream areas would seriously exacerbate air quality, degrade visibility, affect
66 transportation safety, and do adverse effects on public health during the prevalent
67 seasons of dust storms (Chan et al., 2008; Morman and Plumlee, 2013; Wang et al.,
68 2016). When mineral dusts are deposited onto the Earth's surface, they play a key role
69 in biogeochemical cycles of terrestrial ecosystem or ocean (Okin et al., 2004; Jickells
70 et al., 2005; Shao et al., 2011), as well as alter snow and ice albedo (Aoki et al., 2006;
71 Huang et al., 2011; Wang et al., 2014). Last but not least, dust particles can modulate
72 the Earth's energy budget and drive the climate change directly by scattering and
73 absorption of solar/terrestrial radiation (Charlson et al., 1992; Wang et al., 2010b;
74 Huang et al., 2014), and indirectly by acting as effective cloud condensation nuclei or
75 ice nuclei, influencing the cloud microphysics and precipitation processes
76 (Ramanathan et al., 2001; Rosenfeld et al., 2001; DeMott et al., 2003; Huang et al.,
77 2005, 2006, 2010a; Wang et al., 2010c; Creamean et al., 2013). Numerous studies
78 (Sokolik and Toon, 1999; Lafon et al., 2004, 2006) have confirmed that dust particle
79 is one kind of light absorbing substances, and its mass absorption efficiencies at 325
80 nm (0.06~0.12 m²/g) are about 6 times larger than at 660 nm (0.01~0.02 m²/g), owing
81 to the greater absorbing potential of iron oxides at short wavelengths (Alfaro et al.,
82 2004). However, the way of iron oxides mixed with quartz or clay is complicated and
83 strongly impacts the resulting absorption (Claquin et al., 1998, 1999; Sokolik and
84 Toon, 1999). And these mineralogical studies indicate that a lack of consideration of
85 these mixing mechanisms is a significant limitation of the previous dust absorption
86 computations. Although the absorptive ability of dust is two orders of magnitude
87 lower than for black carbon (Yang et al., 2009), the atmospheric mass loading of the



88 former is the same magnitude larger than that of the latter, leading to the total
89 absorption in solar spectrum comparable to black carbon. Chin et al. (2009) evaluated
90 that dust may account for about 53% of global averaged aerosol absorption optical
91 depth at 550 nm, which undoubtedly changes the aforementioned
92 dust-cloud-precipitation interaction and exerts a significant effect on hydrological
93 cycle of the Earth-atmosphere system.

94 East and Central Asia territories are the major source regions of dust aerosols on
95 Earth, which produce a large amount of dust particles every year that become
96 entrained into the upper atmosphere by cold fronts (Zhang et al., 1997; Huang et al.,
97 2009, 2010a, 2014). They can travel over thousands of kilometers, even across the
98 Pacific Ocean and reach the western coast of North America about one week with the
99 prevailing westerly wind (Husar et al., 2001; Uno et al., 2009, 2011), and then modify
100 the climate and environment over extensive area of Asia-Pacific rim. Thus far, there
101 have been a great deal of fruitful field campaigns for exploring Asian dust (e.g.,
102 U.S.S.R.-U.S., ACE-Asia, ADEC, PACDEX, EAST-AIRC), however, most focus on
103 intensive observation period (Golitsyn and Gillette, 1993; Huebert et al., 2003;
104 Nakajima et al., 2003; Mikami et al., 2006; Huang et al., 2008a; Li et al., 2011) and
105 lack of long-term and quantitative knowledge of dust optical, microphysical
106 characteristics (especially absorption properties) and chemical compositions over
107 these regions. Hence, the absorptive capacity of Asian dust aerosol is still an
108 outstanding issue. The variations of dust optical features in model calculations are
109 closely related to the uncertainties in particle size distribution and prescribing a value
110 for complex refractive index. Whereas the key parameters of Asian dust aerosols in
111 present-day climate models are still prescribed to the predetermined properties of
112 Saharan mineral dust.

113 Wang et al. (2004) inferred the refractive index of pure minerals at Qira in
114 Taklimakan Desert during April 12-14, 2002 via combination of theory calculation
115 and composition analysis of aerosol samples, and showed that the value of imaginary
116 part is 0.00411 at 500 nm, which is consistent with the Central Asian dust of
117 0.004 ± 0.001 (Tadzhikistan Desert; Sokolik and Golitsyn, 1993). Uchiyama et al. (2005)



118 determined the single-scattering albedo (SSA) of Aeolian dust from sky radiometer
119 and in situ measurements, and concluded that unpolluted Aeolian dust (source from
120 Taklimakan Desert) has low absorption (with SSA_{500} of 0.93~0.97). Kim et al. (2004)
121 analyzed multiyear sky radiation measurements over East Asian sites of
122 Skyradiometer Network (Nakajima et al., 1996; Takamura et al., 2004) and showed
123 the SSA_{500} of dust particles are around 0.9 in arid Dunhuang of northwest China and
124 Mandalgoi Gobi desert in Mongolia. Bi et al. (2014) also reported the similar SSA_{550}
125 (0.91~0.97) of dust aerosol at Dunhuang during spring of 2012. Xu et al. (2004)
126 gained SSA_{530} of 0.95 ± 0.05 in Yulin, China, from a Radiance Research nephelometer
127 and a Particle Soot Absorption Photometer (PSAP) and suggested that both desert dust
128 and local pollution sources contributed to the aerosol loading in Yulin during April
129 2001. Whereas Ge et al. (2010) examined dust aerosol optical properties at Zhangye
130 (a semiarid area of northwest China) from multifilter rotating shadowband radiometer
131 (MFRSR) during spring of 2008 and found that although there are low aerosol optical
132 depth values (AOD_{670} ranging from 0.07~0.25), dust particles have strong absorption
133 (with SSA_{500} of 0.75 ± 0.02) due to mixing with local anthropogenic pollutants. This
134 result is close to the New Delhi over India (0.74~0.84 for SSA_{500} ; Pandithurai et al.,
135 2008). Lafon et al. (2006) revealed that due to containing of less calcite and higher
136 fraction of iron oxide-clay aggregates, mineral dusts in Niger (Banizoumbou, $13^{\circ}31'N$,
137 $2^{\circ}38'E$) have much lower SSA in the visible wavelengths than that of Chinese (Ulan
138 Buh, $39^{\circ}26'N$, $105^{\circ}40'E$) and Tunisian (Maouna, $33^{\circ}01'N$, $10^{\circ}40'E$) desert locations.
139 Therefore, complete clarification of the climate-relevant impacts of Asian dust
140 aerosols requires extensive and long-term measurements of the optical, microphysical
141 and chemical properties, along with their spatial and temporal distributions.

142 In this paper, we investigate optical characteristics of Asian dust from multi-year
143 AErosol RObotic NETwork (AERONET) measurements at 13 sites in and around arid
144 or semi-arid regions of East and Central Asian desert sources. The key quantities
145 include single-scattering albedo (SSA), asymmetry factor (ASY), real part (Re) and
146 imaginary part (Ri) of complex refractive index, volume size distribution (dV/dlnr),
147 which are needed for climate simulating and remote sensing applications. We mainly



148 compare the vital absorption and optical properties between pure and transported
149 anthropogenic dust over East and Central Asia. This article is arranged as follows.
150 Section 2 introduces the site description and measurement. The identification method
151 and detailed Asian dust optical features are described in Section 3. Discussion of
152 spectral absorption behaviors of different dust aerosol types are given in Section 4 and
153 followed by the Summary in Section 5.

154 **2. Site Description and Measurement**

155 **2.1. Site Description**

156 In this article, we select 13 AERONET sites located in arid or semi-arid Asian
157 regions (see Fig. 1), which are recognized as the primarily active centre of dust storms.
158 These drylands are very sensitive to climate change and human activities and would
159 accelerate drought expansion by the end of twenty-first century (Huang et al., 2016).
160 Eight sites over East Asian region are labeled with red colors, and five sites over
161 Central Asian area are labeled with blue colors. The major Great deserts or Gobi
162 deserts along with plateaus are marked with black font (e.g., Great Gobi desert in
163 Mongolia, Taklimakan Desert, Thar Desert, Karakum Desert, Tibetan Plateau, Loess
164 Plateau, and Iranian Plateau). In order to quantitatively explore detailed spectral
165 absorptive characteristics of dust aerosols over East and Central Asia, we choose four
166 East Asian sites (SACOL, Dalanzadgad, Beijing, and Yulin) and four Central Asian
167 sites (Dushanbe, Karachi, Kandahar, and IASBS). They consist of: SACOL located
168 over Loess Plateau of northwest China (Huang et al., 2008b; Guan et al., 2009; Huang
169 et al., 2010b; Wang et al., 2010a), Dalanzadgad in the Great Gobi of southern
170 Mongolia (Eck et al., 2005), Beijing in the downwind of Inner Mongolia (Xia et al.,
171 2007), Yulin on the southwestern fringe of the Mu Us desert in northwest China (Xu
172 et al., 2004; Che et al., 2009, 2015), Dushanbe in Tadzhikistan situated at the transport
173 corridor of Central Asian desert dust (i.e. Karakum Desert; Golitsyn and Gillette,
174 1993), Karachi located in the southern margin of Thar Desert in Pakistan and about 20
175 km from the east coast of Arabian Sea (Alam et al., 2011), Kandahar in the arid area
176 of southern Afghanistan, IASBS on the Iranian Plateau of northwest Iran.



177 **2.2. Sun Photometer Measurements**

178 AERONET is an internationally federated global ground-based aerosol monitoring
179 network utilizing Cimel sun photometer, which comprises more than 500 sites all over
180 the world (Holben et al., 1998). The Cimel Electronique sun photometer (CE-318)
181 takes measurements of sun direct irradiances at multiple discrete channels within the
182 spectral range of 340-1640 nm, which can be calculated aerosol optical depth (AOD)
183 and columnar water vapor content (WVC) in centimeter. Furthermore, the instrument
184 can perform angular distribution of sky radiances at 440, 675, 870, and 1020 nm
185 (nominal wavelengths), which can be simultaneously retrieved aerosol volume size
186 distribution, complex refractive index, single-scattering albedo, and asymmetry factor
187 under cloudless condition (Dubovik and King, 2000; Dubovik et al., 2002a, 2006).
188 The total accuracy in AOD for a newly calibrated field instrument is about
189 0.010-0.021 (Eck et al., 1999). The retrieval errors of SSA, ASY, Ri, and Re are
190 anticipated to be 0.03-0.05, 0.04, 30%-50%, and 0.025-0.04, respectively, relying on
191 aerosol types and loading (Dubovik et al., 2000). It should be borne in mind that these
192 uncertainties are dependent on $AOD_{440} \geq 0.4$ and for solar zenith angle $> 50^\circ$ (Level 2.0
193 product), and the retrieval errors will become much greater when $AOD_{440} < 0.4$. The
194 datasets of selected 13 AERONET sites in this study come from the Level2.0 product,
195 which are pre- and post-field calibrated, automatically cloud screened, and
196 quality-assured (Smirnov et al., 2000). In addition, a mixture of randomly oriented
197 polydisperse spheroid particle shape assumption with a fixed aspect ratio distribution
198 is applied to retrieve key optical properties of Asian dust (Dubovik, et al., 2002a,
199 2006).

200 **3. Asian Dust Optical properties**

201 A great amount of publications have verified that mineral dust aerosols are
202 commonly predominant by large particles with coarse mode (radii $> 0.6 \mu\text{m}$), which are
203 the essential feature differentiating the dust from fine-mode dominated biomass
204 burning and urban-industrial aerosols (Dubovik et al., 2002b; Eck et al., 2005; Bi et
205 al., 2011, 2014; Kim et al., 2011). In other word, the values of Ångström exponent at



440-870 nm (α) for dust aerosols usually range between -0.1 to 0.6. As pointed out by Smirnov et al. (2002) and Dubovik et al. (2002b), sea salt aerosol is also dominant by coarse mode and has small Ångström exponent ($\sim 0.3-0.7$) but with low AOD_{440} ($\sim 0.15-0.2$) compared to dust aerosol. Moreover, the selected desert locations in this study are mostly not affected by sea salt. By virtue of these differences, we can distinguish Asian dust aerosols from other fine-mode dominated non-dust particles. The criteria of two thresholds are put forward. (I) The particles with high aerosol optical depth at 440 nm ($\text{AOD}_{440} \geq 0.4$) and low Ångström wavelength exponent at 440-870 nm ($\alpha < 0.2$) are defined as Pure Dust (PDU) that keep high accuracy of pure Asian dust and eliminate most fine mode aerosols. (II) The particles with $\text{AOD}_{440} \geq 0.4$ and $0.2 < \alpha < 0.6$ are designated as Transported Anthropogenic Dust (TDU), which are mainly dominated by dust and might mix with other anthropogenic aerosol types during transportation. The definition of anthropogenic dust in this study is different from earlier literatures (Tegen and Fung, 1995; Prospero et al., 2002; Huang et al., 2015), which define that anthropogenic dust is primarily produced by various human activities on disturbed soils (e.g., agricultural practices, industrial activity, transportation, desertification and deforestation). It is still a huge challenge to discriminate between natural and anthropogenic components of dust aerosols by using current technology, AERONET products or in-situ measurements. Recently, Ginoux et al. (2012) first estimated that anthropogenic sources globally account for 25% based on Moderate Resolution Imaging Spectroradiometer (MODIS) Deep Blue dust optical depth in conjunction with other land use data sets. Huang et al. (2015) proposed a new algorithm for distinguishing anthropogenic dust from natural dust by using Cloud-Aerosol Lidar and Infrared Pathfinder Satellite Observation (CALIPSO) and planetary boundary layer (PBL) height retrievals along with MODIS land cover data set. They revealed that anthropogenic dust produced by human activities mainly comes from semi-arid and semi-humid regions and is generally mixed with other types of aerosols within the PBL that is more spherical than natural dust. Thereby, we assume that anthropogenic dust aerosol originated from Asian arid or semi-arid areas has got smaller size distribution (thus larger Ångström exponent) than that of pure



236 natural dust.

237 Before insight into dust aerosol optical characteristics, we first analyze the
238 occurrence frequency of Asian dust over the study region that significantly affects the
239 intensity and distribution of mineral dust loading. Figure 2 depicts the total number
240 days of each month for Pure Dust ($\alpha < 0.2$) and transported Anthropogenic Dust
241 ($0.2 < \alpha < 0.6$) at selected four East Asian sites and four Central Asian sites. The dust
242 events at four East Asian sites primarily concentrate on springtime and corresponding
243 peak days for PDU and TDU both appear in April. This is greatly attributed to the
244 intrusion of dust particles during spring when dust storms are prevalent over these
245 regions (Wang et al., 2008). For SACOL and Beijing sites, both the PDU and TDU
246 days also occur in whole year except for autumn when is the rainy season, which is
247 linked to long-range transport of dust particulates from desert source areas and locally
248 anthropogenic dust (e.g., agricultural cultivation, overgrazing, desertification,
249 industrial and constructed dust in urbanization). Shen et al. (2016) have demonstrated
250 that urban fugitive dust generated by road transport and urban construction
251 contributes to more than 70% of particulate matter ($PM_{2.5}$) in northern China. The
252 dust episodes in Dushanbe of Tadzhikistan mostly happen from July to October,
253 which are the peak seasons of dust storms (Golitsyn and Gillette, 1993). For Karachi
254 site in Pakistan, the dust activities take place in spring and summer seasons. This is
255 because the region is not affected by the summer monsoon, leaving the land surface
256 sufficiently dry, and hence susceptible to wind erosion by strong winds and
257 meso-scale thunderstorm events typical of this time of year (Alizadeh Choobari et al.,
258 2014). In addition, the transport of summer dust plumes from the Arabian Peninsula
259 can partially contribute dust particles to Karachi site. Note that the occurred months of
260 PDU days are nearly different from TDU days at Dalanzadgad, Kandahar, and IASBS
261 sites, suggesting that dust aerosols over these areas are rarely affected by
262 anthropogenic pollutants. For Kandahar site in Afghanistan, the limited sampling days
263 to some extent may affect the statistical results. Generally, the aforementioned
264 occurrence frequency of dust storms over diverse sites are principally dependent on
265 different climatic regime and synoptic pattern, for instance, geographical location,



266 atmospheric circulation, wet season and dry season.

267 Table 1 summarizes the site information, sampling period, overall average optical
268 properties at 550 nm (e.g., SSA, ASY, Re, Ri, and Ångström exponent at 440-870 nm)
269 for Asian PDU ($\alpha < 0.2$), and total number of PDU and TDU ($0.2 < \alpha < 0.6$) days. Note
270 that dust optical feature at a common 550 nm wavelength is utilized here, which can
271 be derived from logarithmic interpolation between 440 and 675 nm. It is worth
272 pointing out that the absorption and optical properties of dust aerosols at two
273 Dunhuang sites exhibit consistent features despite of different sampling periods,
274 which indicate that the chemical composition of dust aerosol at Dunhuang area
275 remains relatively stable.

276 The SSA or Ri of complex refractive index can characterize the absorptive
277 intensity of dust aerosols, and determine the sign (cooling or heating, depending on
278 the planetary albedo) of the radiative forcing (Hansen et al., 1997). Both two
279 quantities are mainly relied on the ferric oxide content in mineral dust (Sokolik and
280 Toon, 1999). Figure 3 illustrates the overall average spectral behavior of key optical
281 properties for PDU ($\alpha < 0.2$) and TDU ($0.2 < \alpha < 0.6$) at selected four East Asian sites.
282 The SSA, ASY, Re and Ri of complex refractive index as a function of wavelength
283 (440, 675, 870, and 1020 nm) are presented. For all cases, the spectral behaviors of
284 aerosol optical parameters exhibit similar features, which can be representative of
285 typical patterns of Asian dust. The SSA values systematically increase with
286 wavelength at 440-675 nm and keep almost neutral or slight increase for the
287 wavelengths greater than 675 nm, which is consistent with the previous results of dust
288 aerosols (Dubovik et al., 2002b; Eck et al., 2005; Bi et al., 2011). In contrast, an
289 opposite pattern is displayed by imaginary part of refractive index, namely, Ri values
290 dramatically decrease from 440 nm to 675 nm, and preserve invariant from 675 nm to
291 1020 nm. These variations indicate that Asian dust aerosols have got much stronger
292 absorptive ability at shorter wavelength. Alfaro et al. (2004) implied that the
293 absorption capacity of soil dust increase linearly with iron oxide content, and
294 estimated SSA at 325 nm (~0.80) is much lower than at 660 nm (~0.95). Sokolik and
295 Toon (1999) revealed that ferric iron oxides (e.g., hematite and goethite) are often



internally mixed with clay minerals and result in significant dust absorption in the UV/visible wavelengths. Hence, the spectral variations of SSA and Ri with wavelengths are attributable to the domination of coarse-mode dust particles that have larger light absorption in the blue spectral band as mentioned above. It is worth noting that spectral ASY values remarkably reduce from 440 nm to 675 nm, and are almost constant at 675-1020 nm range. This suggests that Asian dust aerosols have much stronger scattering at 440 nm than other longer visible wavebands, due to the contribution of coarse mode particles. By contrast, the spectral behavior of Re is not obvious for PDU and TDU at all sites, and the mean Re values at 440 nm vary between 1.50 and 1.56. Although there are 18 years continuous AERONET datasets at Dalanzadgad site, the effective days of PDU and TDU are only 8 and 6 days, respectively, almost appearing in springtime period. There are no identifiable differences for dust absorption properties between PDU and TDU cases for Dalanzadgad, which indicates again that the site is hardly influenced by anthropogenic pollutants. The spectral discrepancies of optical characteristics between PDU and TDU at other three sites show much more apparent than Dalanzadgad, which is ascribed to these regions are not only affected by dust aerosols, but also including local anthropogenic emissions, for instance, urban-industry, coal fuel combustion, biomass burning, mobile source emissions, and agricultural dust (Xu et al., 2004; Xia et al., 2007; Che et al., 2015; Bi et al., 2011; Wang et al., 2015).

Figure 4 is the same as Figure 3, but for selected four Central Asian sites. The wavelength dependencies of PDU and TDU cases at Central Asian sites are consonant with that of East Asian sites, despite of somewhat different variations of magnitude and amplitude. This is expected, because the East Asian desert sites are very close to the Central Asian desert locations and remain similar chemical compositions of dust aerosols (Wang et al., 2004). The spectral behaviors of dust optical properties for PDU at Kandahar and IASBS sites are nearly the same as TDU cases, which agrees well with the consistent variability of occurrence of dust storms. The wavelength dependency of dust characteristics for PDU at Dushanbe and Karachi presents large differences with TDU case, which is also likely due to the influence of local



326 anthropogenic pollutions. Furthermore, the standard deviation of PDU is far less than
327 that of TDU at all wavelengths, suggesting that the robustness of PDU recognition
328 method.

329 Particle size distribution is another critical agent for deciding the optical and
330 radiative properties of dust aerosol. Nakajima et al. (1996) and Dubovik and King
331 (2000) uncovered that based on the spherical Mie theory, the retrieval errors of
332 volume size distribution do not exceed 10% for intermediate particle size ($0.1 \leq r \leq 7$
333 μm) and may greatly increase to 35-100% at the edges of size range ($r < 0.1 \mu\text{m}$ or $r > 7$
334 μm). As mentioned above, a polydisperse, randomly oriented spheroid method is
335 utilized in this study, which is demonstrated to remove the artificially increased size
336 distribution of fine particle mode with $\text{AOD}_{440} \geq 0.4$ and for solar zenith angle $> 50^\circ$.
337 Additionally, the large errors at the edges do not significantly affect the derivation of
338 the main features of the particle size distribution (concentration, median and effective
339 radii, etc.), because typical dust aerosol size distributions have low values at the edges
340 of retrieval size interval (Dubovik et al., 2002a). Figure 5 delineates the overall
341 average columnar aerosol volume size distributions ($dV/dlnr$, $0.05 \mu\text{m} \leq r \leq 15 \mu\text{m}$) for
342 Pure Dust ($\alpha < 0.2$) and Transported Anthropogenic Dust ($0.2 < \alpha < 0.6$) at selected 13
343 AERONET sites. Corresponding AOD_{440} and effective radius of coarse mode (r_{coarse})
344 in μm are also shown. It is apparent that the $dV/dlnr$ exhibits a typical bimodal
345 structure and is dominant by coarse mode for PDU and TDU at all sites. The $dV/dlnr$
346 peak of coarse mode particle varies dramatically and appears at a radius $r_{Vc} \sim 2.24 \mu\text{m}$
347 for all PDU and TDU cases, while the corresponding peak of fine mode particle arises
348 at a radius $r_{Vf} \sim 0.09-0.12 \mu\text{m}$. The $dV/dlnr$ peak and effective radius (r_{coarse}) of coarse
349 mode particles strikingly increase with the increase of AOD ascribed to the intrusion
350 of dust particles. For instance, the AOD_{440} , $dV/dlnr$ peak values of coarse mode, and
351 r_{coarse} for PDU at Minqin site are 0.48, $0.31 \mu\text{m}^3/\mu\text{m}^2$, and $1.74 \mu\text{m}$, respectively, and
352 corresponding values are 1.13, $0.77 \mu\text{m}^3/\mu\text{m}^2$, and $1.93 \mu\text{m}$ at Lahore site, as shown
353 in Fig. 5(a). The average volume median radii of fine-mode and coarse-mode particles
354 for PDU are $0.159 \mu\text{m}$ and $2.157 \mu\text{m}$, respectively, and $0.140 \mu\text{m}$ and $2.267 \mu\text{m}$ for
355 TDU (see Table. 2). The mean volume concentration ratio of coarse mode to fine



356 mode particles (C_{vc}/C_{vf}) for Pure Dust is about 18 (varying between 11~31) over East
357 and Central Asia, which is close to the average of ~20 at Dunhuang_LZU during the
358 spring of 2012 (Bi et al., 2014), and much less than that over Saharan pure desert
359 domain (~50) (Dubovik et al., 2002b). The $dV/dlnr$ peak of coarse mode for TDU is
360 clearly smaller than that for PDU, and corresponding mean C_{vc}/C_{vf} value is 9 (~5-11).
361 We attribute the high fractions of coarse-mode particles to high AOD and low
362 Ångström exponent values.

363 In this paper, we postulate that Asian dust particles only possess scattering and
364 absorption characteristics. And the absorption AOD value (AAOD) at a specific
365 wavelength can be obtained from SSA and AOD, namely, $AAOD_{\lambda} = (1-SSA_{\lambda}) \times AOD_{\lambda}$,
366 where λ is the wavelength. Thereby, the corresponding absorption Ångström exponent
367 at 440-870 nm (AAE) is calculated from spectral AAOD values by using a log-linear
368 fitting algorithm. Figure 6 outlines the total average Ångström exponent (α) and
369 absorption Ångström exponent at 440-870 nm, volume concentration of coarse mode
370 in $\mu\text{m}^3/\mu\text{m}^2$, and volume median radius of coarse mode in μm for TDU ($0.2 < \alpha < 0.6$)
371 and PDU ($\alpha < 0.2$) at selected AERONET sites. There are very big differences of all
372 quantities between PDU and TDU cases, except for some sites (e.g., Dunhuang and
373 Minqin). The primary reason is that we only acquire limited datasets of dust days
374 during spring time at Dunhuang and Minqin sites, which are hardly affected by other
375 anthropogenic pollutants. The AE values of TDU show remarkable changes among
376 each site, ranging from 0.24 to 0.44, whereas corresponding values of PDU keep
377 comparatively slight variations for selected 13 sites (~0.04-0.15). Furthermore, all the
378 AAE values of PDU are greater than 1.5, ranging between 1.65 and 2.36, and the
379 AAE of TDU vary from 1.2 to 2.3. We can conclude that the Asian pure dust aerosols
380 have got AE values smaller than 0.2 and corresponding AAE larger than 1.50, which
381 is another typical feature distinguishing with other non-dust aerosols. Yang et al.
382 (2009) attributed the high AAE values of dust aerosol in China to the presence of
383 ferric oxides. It is evident that volume concentrations of coarse mode for PDU are
384 significantly higher than TDU case, which is expected for the more coarse-mode
385 particles in PDU. While the volume median radius of coarse mode for TDU is greater



386 than PDU case, although there are some smaller values for TDU at Dalanzadgad and
387 Yulin sites. This is owing to dust particles at these sites usually mix with other
388 anthropogenic aerosol species and substantially enhance their median radii.

389 Figure 7 characterizes the overall mean optical properties (e.g., SSA, ASY, Re,
390 and Ri) at 440 nm for selected 13 sites. In general, the absorption capacity of PDU is
391 less than that for TDU. That is, higher SSA and smaller Ri values for PDU, except for
392 Dalanzadgad site. A reasonable interpretation is that threshold criterion method for
393 PDU in this study has effectively eliminated the fine mode aerosols, which are mostly
394 the much stronger absorbing aerosols (e.g., soot and biomass burning aerosol) over
395 East and Central Asia but weaker absorbing pollution aerosols (i.e., sulfate and nitrate)
396 over Dalanzadgad. Wu et al. (2012, 2014) have documented that sulfate and nitrate in
397 background atmosphere most likely originated directly from surface soil at the north
398 and south edges of Taklimakan desert and comprised steadily about 4% of dust
399 particulate matters, which could partially explain our results. Additionally, the overall
400 mean ASY and Re of PDU are greater than that of TDU, which again verifies that the
401 Asian pure dust has got much stronger forward scattering ability than the mixture of
402 Asian dust. Note that the standard deviation of SSA and Ri for PDU is a factor of two
403 to four lower than those from TDU. And the total average values of SSA, ASY, Re,
404 and Ri at 550 nm wavelength for Asian PDU are 0.935 ± 0.014 , 0.742 ± 0.008 ,
405 1.526 ± 0.029 , and 0.00226 ± 0.00056 , respectively, while corresponding values are
406 0.921 ± 0.021 , 0.723 ± 0.009 , 1.521 ± 0.025 , 0.00364 ± 0.0014 for TDU. Yang et al. (2009)
407 took advantage of various in situ aerosol optical and chemical measurements at
408 Xianghe, China during the EAST-AIRC campaign, and deduced a refractive index of
409 $1.53 - 0.0023i$ at 550 nm of dust aerosol, which is close to the result of PDU in this
410 study. Nevertheless, the TDU case should be much closer to actual airborne dust
411 aerosol in the real world. When the elevated dusts over desert source regions are
412 transported eastward, they generally mix with other chemical species and react
413 heterogeneously with anthropogenic pollutants, and thus may significantly modify
414 their chemical composition and microphysical properties (Arimoto et al., 2004).
415 Recently, Kim et al. (2011) presented that the annual mean SSA, ASY, Re, and Ri of



416 complex refractive index for nearly pure Saharan dust are 0.944 ± 0.005 , 0.752 ± 0.014 ,
417 1.498 ± 0.032 , and 0.0024 ± 0.0034 at 550 nm, respectively, which are close to our
418 results of pure Asian dust but exist some differences of quantitative values and
419 spectral behaviors.

420 Average spectral optical properties (at 440, 675, 870, and 1020 nm) for PDU and
421 TDU over East and Central Asian regions are tabulated in Table 2. To our knowledge,
422 this is the first built on Asian dust optical characteristics utilizing multiyear and
423 multi-site AERONET measurements, which will hopefully improve uncertainties of
424 Asian dust shortwave radiative forcing in current regional and global climate models.

425 **4. Discussion**

426 Figure 8 describes the mean spectral behaviors of Re, RI, and SSA for Asian Pure
427 Dust ($\alpha<0.2$) in this study along with published dust results over various geographical
428 locations (Carlson and Caverly, 1977 or C77; Patterson et al., 1977 or P77; WMO,
429 1983; Hess et al., 1998 or OPAC; Dubovik et al., 2002b or Persian Gulf; Alfaro et al.,
430 2004 or Ulan Buh Desert; Wang et al., 2004 or ADEC; Todd et al., 2007 or T07). It is
431 well known that a lot of present-day dust models commonly take advantage of the
432 Optical Properties of Aerosols and Clouds (OPAC, Hess et al., 1998) or World
433 Meteorological Organization (WMO, 1983) databases. Curves C77 and P77 show the
434 complex refractive index of Saharan dust in Cape Verde Islands, Barbados West
435 Indies, Tenerife Canary Islands obtained from laboratory analysis by Carlson and
436 Caverly (1977) and Patterson et al. (1977), respectively. Curve P77 gives one of the
437 most widely used datasets of Ri value in the range 300-700 nm. Curve Persian
438 Gulf(98-00) displays the refractive index and SSA of dust over Bahrain-Persian Gulf
439 Desert during period of 1998-2000 derived from Dubovik et al. (2002b). Curve T07
440 shows the optical properties of mineral dust over Bodélé Depression of northern Chad
441 during 2005 retrieved from Cimel sun photometer by Todd et al. (2007). And the
442 curves ADEC and Ulan Buh exhibit the dust absorptive properties over
443 aforementioned Taklimakan Desert and Ulan Buh Desert of northwest China by Wang
444 et al. (2004) and Alfaro et al. (2004). Figure 8(a) presents that the spectral behaviors



445 of Re have relatively slight variations with values ranging from 1.50-1.56 apart from
446 T07 that shows lower Re values of 1.44-1.47. Todd et al. (2007) utilized Scanning
447 Electron Microscope (SEM) analysis of airborne dust material and confirmed that the
448 mineral dust is dominated by fragmented fossil diatoms from the dry lake bed of the
449 Bodélé Depression, which is to some extent different from the typical desert soil. As
450 shown in Figure 8(b), wavelength dependences of Ri exhibit comparably greater
451 differences in UV wavebands. In mid-visible and near infrared, our results are slightly
452 larger than Persian Gulf (98-00) and T07 that are retrieved from Cimel sun
453 photometer, but still comparable. It is very distinct that the absorbing ability of Asian
454 pure dust ($\alpha < 0.2$) in the whole spectrum range is about a factor of 4 smaller than
455 current dust models (WMO, 1983; Hess et al., 1998), and is a factor of 2 to 3 lower
456 than the results from in situ measurements combined with laboratory analysis or
457 model calculations (Carlson and Caverly, 1977; Patterson et al., 1977; Wang et al.,
458 2004). Meanwhile, the wavelength dependences of SSA agree well with Persian Gulf
459 (98-00) and Ulan Buh Desert, but are much higher than OPAC. The discrepancy
460 increases dramatically with decreasing wavelength. Such big differences of dust
461 absorption capacity for diverse dust models (OPAC and WMO) and researches will
462 certainly lead to different radiative impacts on regional or global climate change.

463 Figure 9 draws the aerosol shortwave direct radiative effects (ARF) at the top of
464 atmosphere (TOA), at the surface (SFC), and in the atmospheric layer (ATM) for
465 Asian Pure Dust ($\alpha < 0.2$) and Transported Anthropogenic Dust ($0.2 < \alpha < 0.6$) acquired
466 in this study, and corresponding ARF values for OPAC Mineral accumulated (Mineral
467 acc.) and transported (Mineral tran.) modes are also presented for comparison. We
468 make use of the Santa Barbara Discrete-ordinate Atmospheric Radiative Transfer
469 model (SBDART, Ricchiazzi et al., 1998) to calculate the ARF, which has been
470 proved to be a reliable software code and widely used for simulating plane-parallel
471 radiative fluxes in the Earth's atmosphere (Halthore et al., 2005; Bi et al., 2013). The
472 main input parameters of spectral AOD, surface albedo, WVC, and columnar ozone
473 amount are prescribed to same values, and the spectral SSA, ASY, Re, and Ri values
474 are obtained from aforementioned various dust models. It is evident that Earth's



475 energy budget is modulated and redistributed by different absorbing properties of
476 mineral dusts. The results indicate that the cooling rate at SFC (negative radiative
477 forcing) gradually increases with PDU ($\alpha < 0.2$), TDU ($0.2 < \alpha < 0.6$), OPAC Mineral
478 accumulated and transported dust modes. By contrast, the cooling intensity at TOA
479 gradually decreases with diverse dust cases, and even becomes positive radiative
480 forcing for OPAC transported dust mode, with ARF varying from -15.6, -13.8, -6.9,
481 and +0.24 W m^{-2} , respectively. Therefore, the heating intensity in the atmospheric
482 layer sharply increases from +22.7, +29.5, +46.6, and +58.3 W m^{-2} . The heating rate in
483 ATM for OPAC Mineral (acc. and tran.) modes is about two-fold greater than Asian
484 dust cases (PDU and TDU). Such large diabatic heating rates might warm the dust
485 layer, suppress the development of convection under the lower atmosphere, thus exert
486 profound impacts on the atmospheric dynamical and thermodynamic structures and
487 cloud formation together with the strength and occurrence frequency of precipitation
488 (Rosenfeld et al., 2001; Huang et al., 2010a; Creamean et al., 2013). Hence, accurate
489 and reliable absorbing characteristics of Asian dust should be considered in
490 present-day regional climate models.

491 **5. Summary**

492 In this study, we have proposed two threshold criteria to discriminate two types of
493 Asian dust: Pure Dust (PDU, $\alpha < 0.2$) and Transported Anthropogenic Dust (TDU,
494 $0.2 < \alpha < 0.6$). PUD can represent nearly “pure” dust in desert source regions and
495 decrease disturbance of other non-dust aerosols, which would also exclude some fine
496 mode of dust particles. The spectral behaviors of TDU exhibit similar variations with
497 PDU, but show much stronger absorption and weaker scattering than PDU cases.
498 There are two markedly identifiable characteristics for Asian PDU. (I) spectral SSA
499 values systematically increase with wavelength from 440 nm to 675 nm and remain
500 almost neutral or slight increase for the wavelength greater than 675 nm, whereas an
501 opposite pattern is shown for imaginary part of refractive index. (II) Asian pure dust
502 aerosols have got AE values smaller than 0.2 and AAE larger than 1.50. Compared
503 with current common dust models (e.g., OPAC and WMO), Asian dust aerosol has



504 relatively weak absorption for wavelengths greater than 550 nm (SSA~0.96-0.99), but
505 presents a moderate absorption in the blue spectral range (SSA₄₄₀~0.92-0.93). The
506 overall average values of SSA, ASY, Re, and Ri at 550 nm wavelength for Asian PDU
507 are 0.935±0.014, 0.742±0.008, 1.526±0.029, and 0.00226±0.00056, respectively,
508 while corresponding values are 0.921±0.021, 0.723±0.009, 1.521±0.025,
509 0.00364±0.0014 for TDU.

510 It should be noted that the definition of anthropogenic dust in this paper is
511 ambiguous, and TDU here represents more accurately dominant dust mixing with
512 other anthropogenic aerosols. Because it is very difficult to quantify the
513 anthropogenic contribution due to large uncertainties in defining the anthropogenic
514 fraction of ambient dust burden (Sokolik et al., 2001; Huang et al., 2015). Diverse
515 human activities (e.g., agricultural cultivation, desertification, industrial activity,
516 transportation, and construction in urbanization) in vulnerable environments might
517 modify the land use and Earth's surface cover, and would affect the occurred
518 frequency and intensity of anthropogenic dust. Hence, the optical features of
519 anthropogenic dust aerosols are dependent on the source regions and chemical
520 compositions. However, as concluded by Huang et al. (2015), anthropogenic dust
521 generated by human activities mainly comes from semi-arid and semi-humid regions
522 (Guan et al., 2016) and is generally mixed with other types of aerosols within the PBL.
523 And we primarily investigated dust aerosols in arid or semi-arid regions over East and
524 Central Asia, where are somewhat disturbed by human activities. Therefore, the key
525 optical properties of TDU derived from this study should to some extent contain the
526 anthropogenic fraction. To fully elucidate exact optical properties of anthropogenic
527 dust, we need to explore detailed morphology, mineralogy, and chemical
528 compositions by means of in situ measurements, laboratory analysis, active and
529 passive remote sensing methods (e.g., multi-wavelength lidar, AEROENT, MODIS)
530 as well as model calculations.

531
532 *Acknowledgements.* This work was jointly supported by the National Science Foundation of
533 China (41521004, 41305025, 41575015 and 41405113), the Fundamental Research Funds for the



534 Central Universities lzujbky-2015-4 and lzujbky-2013-ct05, and the China 111 Project (No. B
535 13045). We thank the GSFC/NASA AERONET group for processing the AERONET data
536 (<http://aeronet.gsfc.nasa.gov>). The authors would like to express special thanks to the
537 principal investigators (Hong-Bin Chen, Philippe Goloub, Bernadette Chatenet, Xiao-Ye Zhang,
538 Laurent Gomes, Sabur F. Abdullaev, and Hamid Khalesifard) and their staff for effort in
539 establishing and maintaining the instruments at AERONET sites used in this work. We appreciate
540 the MODIS and TOMS teams for supplying the satellite data. We would also like to thank all
541 anonymous reviewers for their constructive and insightful comments.

542

543

544 **References**

545 Alam, K., Trautmann, T., and Blaschke, T.: Aerosol optical properties and radiative forcing over
546 mega-city Karachi, *Atmos. Res.*, 101, 773-782, doi:10.1016/j.atmosres.2011.05.007, 2011.

547 Alfaro, S. C., Lafon, S., Rajot, J. L., Formenti, P., Gaudichet, A., and Maillé, M.: Iron oxides and
548 light absorption by pure desert dust: An experimental study, *J. Geophys. Res.*, 109, D08208,
549 doi:10.1029/2003JD004374, 2004.

550 Alizadeh Choobari, O., Zawar-Reza, P., and Sturman, A.: The global distribution of mineral dust
551 and its impacts on the climate system: A review, *Atmos. Res.*, 138, 152-165,
552 doi:10.1016/j.atmosres.2013.11.007, 2014.

553 Aoki, T., Motoyoshi, H., Kodama, Y., Yasunari, T. J., Sugiura, K., and Kobayashi, H.:
554 Atmospheric aerosol deposition on snow surfaces and its effect on albedo, *SOLA*, 2, 13-16,
555 doi:10.2151/sola.2006-004, 2006.

556 Arimoto, R., X. Y. Zhang, B. J. Huebert, C. H. Kang, D. L. Savoie, J. M. Prospero, S. K. Sage, C.
557 A. Schloesslin, H. M. Khaing, and S. N. Oh: Chemical composition of atmospheric aerosols
558 from Zhenbeitai, China, and Gosan, South Korea, during ACE-Asia, *J. Geophys. Res.*, 109,
559 D19S04, doi:10.1029/2003JD004323, 2004.

560 Bi, J., Huang, J., Fu, Q., Wang, X., Shi, J., Zhang, W., Huang, Z., and Zhang B.: Toward
561 characterization of the aerosol optical properties over Loess Plateau of Northwestern China, *J.*
562 *Quant. Spectrosc. Radiat. Transfer.*, 112, 346-360, doi:10.1016/j.jqsrt.2010.09.006, 2011.



563 Bi, J., Huang, J., Fu, Q., Ge, J., Shi, J., Zhou, T., and Zhang, W.: Field measurement of clear-sky
564 solar irradiance in Badain Jaran Desert of Northwestern China, *J. Quant. Spectroc. Radiat.*
565 *Transf.*, 122, 194-207, doi:10.1016/j.jqsrt.2012.07.025, 2013.

566 Bi, J., Shi, J., Xie, Y., Liu, Y., Takamura, T., and Khatri, P.: Dust aerosol characteristics and
567 shortwave radiative impact at a Gobi Desert of Northwest China during the spring of 2012. *J.*
568 *Meteo. Soc. Jp*, 92A, 33-56, DOI:10.2151/jmsj.2014-A03, 2014.

569 Carlson, T. N. and Caverly, R. S.: Radiative characteristics of Saharan dust at solar wavelengths, *J.*
570 *Geophys. Res.*, 82(21), 3141-3152, 1977.

571 Chan, C. -C., Chuang, K. -J., Chen, W. -J., Chang, W. -T., Lee, C. -T., and Peng, C. -M.:
572 Increasing cardiopulmonary emergency visits by long-range transported Asian dust storms in
573 Taiwan, *Environ. Res.*, 106, 393-400, 2008.

574 Charlson, R. J., Schwartz, S. E., Hales, J. M., Cess, R. D., Coakley Jr., J. A., Hansen, J. E., and
575 Hofmann, D. J.: Climate forcing by anthropogenic aerosols, *Science*, 255, 423-430,
576 doi:10.1126/science.255.5043.423, 1992.

577 Che, H., Zhang, X., Alfraro, S., Chatenet, B., Gomes, L., and Zhao, J.: Aerosol optical properties
578 and its radiative forcing over Yulin, China in 2001 and 2002, *Adv. Atmos. Sci.*, 26(3), 564-576,
579 doi:10.1007/s00376-009-0564-4, 2009.

580 Che, H., Zhang, X.-Y., Xia, X., Goloub, P., Holben, B., Zhao, H., Wang, Y., Zhang, X.-C., Wang,
581 H., Blarel, L., Damiri, B., Zhang, R., Deng, X., Ma, Y., Wang, T., Geng, F., Qi, B., Zhu, J., Yu,
582 J., Chen, Q., and Shi, G.: Ground-based aerosol climatology of China: aerosol optical depths
583 from the China Aerosol Remote Sensing Network (CARSNET) 2002–2013, *Atmos. Chem.*
584 *Phys.*, 15, 7619-7652, doi:10.5194/acp-15-7619-2015, 2015.

585 Chin, M., Diehl, T., Dubovik, O., Eck, T. F., Holben, B. N., Sinyuk, A., and Streets, D. G.: Light
586 absorption by pollution, dust, and biomass burning aerosols: a global model study and
587 evaluation with AERONET measurements, *Ann. Geophys.*, 27, 3439-3464,
588 doi:10.5194/angeo-27-3439-2009, 2009.

589 Clauquin, T., Schulz, M., Balkanski, Y., and Boucher, O.: Uncertainties in assessing radiative
590 forcing by mineral dust, *Tellus Ser. B*, 50, 491-505, 1998.

591 Clauquin, T., Schulz, M., and Balkanski, Y.: Modeling the mineralogy of atmospheric dust sources,
592 *J. Geophys. Res.*, 104, D18, 22243-22256, 1999.



593 Creamean, J. M., Suski, K. J., Rosenfeld, D., Cazorla, A., DeMott, P. J., Sullivan, R. C., White, A.
594 B., Ralph, F. M., Minnis, P., Comstock, J. M., Tomlinson, J. M., and Prather, K. A.: Dust and
595 biological aerosols from the Sahara and Asia influence precipitation in the western U.S.,
596 Science, 339, 1572-1578, doi:10.1126/science.1227279, 2013.

597 DeMott, P. J., Sassen, K., Poellot, M. R., Baumgardner, D., Rogers, D. C., Brooks, S. D., Prenni,
598 A. J., and Kreidenweis, S. M.: African dust aerosols as atmospheric ice nuclei, Geophys. Res.
599 Lett., 30(14), 1732, doi:10.1029/2003GL017410, 2003.

600 Dubovik, O. and King, M. D.: A flexible inversion algorithm for retrieval of aerosol optical
601 properties from Sun and sky radiance measurements, J. Geophys. Res., 105(D16),
602 20673-20696,
603 doi:10.1029/2000JD900282, 2000.

604 Dubovik, O., Smirnov, A., Holben, B. N., King, M. D., Kaufman, Y. J., Eck, T. F., and Slutsker, I.:
605 Accuracy assessments of aerosol optical properties retrieved from Aerosol Robotic Network
606 (AERONET) Sun and sky radianc measurements, J. Geophys. Res., 105(D8), 9791–9806,
607 doi:10.1029/2000JD900040, 2000.

608 Dubovik, O., Holben, B. N., Lapyonok, T., Sinyuk, A., Mishchenko, M. I., Yang, P., and Slutsker,
609 I.: Non-spherical aerosol retrieval method employing light scattering by spheroids, Geophys.
610 Res. Lett., 29(10), 1415, doi:10.1029/2001GL014506, 2002a.

611 Dubovik, O., Holben, B. N., Eck, T. F., Smirnov, A., Kaufman, Y. J., King, M. D., Tanré, D., and
612 Slutsker, I.: Variability of absorption and optical properties of key aerosol types observed in
613 worldwide locations, J. Atmos. Sci., 59, 590–608, 2002b.

614 Dubovik, O., Sinyuk, A., Lapyonok, T. Holben, B. N., Mishchenko, M., Yang, P., Eck, T. F.,
615 Volten, H., Muñoz, O., Veihemann, B., van der Zande, W. J., Leon, J. -F., Sorokin, M., and
616 Slutsker, I.: Application of spheroid models to account for aerosol particle nonsphericity in
617 remote sensing of desert dust, J. Geophys. Res., 111, D11208, doi:10.1029/2005JD006619,
618 2006.

619 Eck, T. F., Holben, B. N., Reid, J. S., Dubovik, O., Smirnov, A., O'Neill, N. T., Slutsker, I., and
620 Kinne, S.: Wavelength dependence of the optical depth of biomass burning, urban and desert
621 dust aerosols, J. Geophys. Res., 104, 31 333-31350, 1999.

622 Eck, T. F., et al.: Columnar aerosol optical properties at AERONET sites in central eastern Asia



623 and aerosol transport to the tropical mid-Pacific, *J. Geophys. Res.*, 110, D06202,
624 doi:10.1029/2004JD005274, 2005.

625 Ge, J., Su, J., Ackerman, T. P., Fu, Q., Huang, J., and Shi, J.: Dust aerosol optical properties
626 retrieval and radiative forcing over northwest China during the 2008 China-U.S. joint field
627 experiment, *J. Geophys. Res.*, 115, D00K12, doi:10.1029/2009JD013263, 2010.

628 Ginoux, P., Prospero, J. M., Gill, T. E., Hsu, N. C., and Zhao, M.: Global-scale attribution of
629 anthropogenic and natural sources and their emission rates based on MODIS Deep Blue aerosol
630 products, *Rev. Geophys.*, 50, RG3005, doi:10.1029/2012RG000388, 2012.

631 Golitsyn, G. and Gillette, D. A.: Introduction: A joint Soviet-American experiment for the study of
632 Asian desert dust and its impact on local meteorological conditions and climate, *Atmos.*
633 *Environ.*, 27A, 16, 2467-2470, 1993.

634 Guan X., Huang, J., Guo, N., Bi, J., and Wang, G: Variability of soil moisture and its relationship
635 with surface albedo and soil thermal parameters over the Loess Plateau, *Adv. Atmos. Sci.*, 26(9),
636 692-700, doi:10.1007/s00376-009-8198-0, 2009.

637 Guan, X., Huang, J., Zhang, Y., Xie, Y., and Liu, J.: The relationship between anthropogenic dust
638 and population over global semi-arid regions, *Atmos. Chem. Phys.*, 16, 5159-5169,
639 doi:10.5194/acp-16-5159-2016, 2016.

640 Halthore, R. N., et al.: Intercomparison of shortwave radiative transfer codes and measurements, *J.*
641 *Geophys. Res.*, 110, D11206, doi:10.1029/2004JD005293, 2005.

642 Hansen, J., Sato, M., and Ruedy, R.: Radiative forcing and climate response, *J. Geophys. Res.*, 102,
643 6831-6864, 1997.

644 Hess, M., Kopke, P., and Schult, I.: Optical properties of aerosols and clouds: The software
645 package OPAC, *Bull. Amer. Meteor. Soc.*, 79, 831-844, 1998.

646 Holben, B. N., Eck, T. F., Slutsker, I., Tanre, D., Buis, J. P., Setzer, A., Vermote, E., Reagan, J. A.,
647 Kaufman, Y. J., Nakajima, T., Lavenu, F., Jankowiak, F., and Smirnov, A., AERONET—A
648 federated instrument network and data archive for aerosol characterization, *Remote Sens.*
649 *Environ.*, 66, 1-16, 1998.

650 Huang, J., Minnis, P., Lin, B., Yi, Y., Khaiyer, M. M., Arduini, R. F., Fan, A., and Mace, G. G.:
651 Advanced retrievals of multilayered cloud properties using multispectral measurements, *J.*
652 *Geophys. Res.*, 110, D15S18, doi:10.1029/2004JD005101, 2005.



653 Huang, J., Lin, B., Minnis, P., Wang, T., Wang, X., Hu, Y., Yi, Y., and Ayers, J. K.: Satellite-based
654 assessment of possible dust aerosols semi-direct effect on cloud water path over East Asia,
655 *Geophys. Res. Lett.*, 33, L19802, doi:10.1029/2006GL026561, 2006.

656 Huang, J., Minnis, P., Chen, B., Huang, Z., Liu, Z., Zhang, Q., Yi, Y., and Ayers, J. K.: Long-range
657 transport and vertical structure of Asian dust from CALIPSO and surface measurements during
658 PACDEX, *J. Geophys. Res.*, 113, D23212, doi:10.1029/2008JD010620, 2008a.

659 Huang, J., Zhang, W., Zuo, J., Bi, J., Shi, J., Wang, X., Chang, Z., Huang, Z., Yang, S., Zhang, B.,
660 Wang, G., Feng, G., Yuan, J., Zhang, L., Zuo, H., Wang, S., Fu, C., and Chou, J.: An overview of
661 the semi-arid climate and environment research observatory over the Loess Plateau, *Adv. Atmos.*
662 *Sci.*, 25, 906-921, doi:10.1007/s00376-008-0906-7, 2008b.

663 Huang, J., Fu, Q., Su, J., Tang, Q., Minnis, P., Hu, Y., Yi, Y., and Zhao, Q.: Taklimakan dust
664 aerosol radiative heating derived from CALIPSO observations using the Fu-Liou radiation
665 model with CERES constraints, *Atmos. Chem. Phys.*, 9, 4011-4021,
666 doi:10.5194/acp-9-4011-2009, 2009.

667 Huang, J., Minnis, P., Yan, H., Yi, Y., Chen, B., Zhang, L., and Ayers, J. K.: Dust aerosol effect on
668 semi-arid climate over Northwest China detected from A-Train satellite measurements, *Atmos.*
669 *Chem. Phys.*, 10, 6863-6872, doi:10.5194/acp-10-6863-2010, 2010a.

670 Huang, J., Fu, Q., Zhang, W., Wang, X., Zhang, R., Ye, H., and Warren, S. G.: Dust and black
671 carbon in seasonal snow across northern China, *Bull. Amer. Meteor. Soc.*, 92, 175-181,
672 doi:10.1175/2010BAMS3064.1, 2011.

673 Huang, J., Wang, T., Wang, W., Li, Z., and Yan, H.: Climate effects of dust aerosols over East
674 Asian arid and semiarid regions, *J. Geophys. Res.*, 119, 11398-11416,
675 doi:10.1002/2014JD021796, 2014.

676 Huang, J. P., Liu, J. J., Chen, B., and Nasiri, S. L.: Detection of anthropogenic dust using
677 CALIPSO lidar measurements, *Atmos. Chem. Phys.*, 15, 11653-11665,
678 doi:10.5194/acp-15-11653-2015, 2015.

679 Huang, J., Yu, H., Guan, X., Wang, G., and Guo, R.: Accelerated dryland expansion under climate
680 change, *Nature Clim. Change*, 6(2), 166-171, doi:10.1038/nclimate2837, 2016.

681 Huang, Z., Huang, J., Bi, J., Wang, G., Wang, W., Fu, Q., Li, Z., Tsay, S.-C., and Shi, J.: Dust
682 aerosol vertical structure measurements using three MPL lidars during 2008 China-U.S. joint



683 dust field experiment, *J. Geophys. Res.*, 115, D00K15, doi:10.1029/2009JD013273, 2010b.

684 Huebert, B. J., Bates, T., Russell, P. B., Shi, G., Kim, Y. J., Kawamura, K., Carmichael, G., and
685 Nakajima, T.: An overview of ACE-Asia: Strategies for quantifying the relationships between
686 Asian aerosols and their climatic impacts, *J. Geophys. Res.*, 108(D23), 8633,
687 doi:10.1029/2003JD003550, 2003.

688 Husar, R. B., Tratt, D. M., and Schichtel, B. A., et al.: Asian dust events of April 1998, *J. Geophys.*
689 *Res.*, 106, D16, 18317-18330, 2001.

690 Jickells, T., An, Z., Andersen, K., Baker, A., Bergametti, G., Brooks, N., Cao, J., Boyd, P., Duce,
691 R., Hunter, K., Kawahata, H., Kubilay, N., laRoche, J., Liss, P., Mahowald, N., Prospero, J.,
692 Ridgwell, A., Tegen, I., and Torres, R.: Global iron connections between desert dust, ocean
693 biogeochemistry, and climate, *Science*, 308, 67-71, doi:10.1126/science.1105959, 2005.

694 Kim, D.-H., Sohn, B. -J., Nakajima, T., Takamura, T., Takemura, T., Choi, B. -C., and Yoon, S. -C.:
695 Aerosol optical properties over east Asia determined from ground-based sky radiation
696 measurements, *J. Geophys. Res.*, 109, D02209, doi:10.1029/2003JD003387, 2004.

697 Kim, D., Chin, M., Yu, H., Eck, T. F., Sinyuk, A., Smirnov, A., and Holben, B. N.: Dust optical
698 properties over North Africa and Arabian Peninsula derived from the AERONET dataset, *Atmos.*
699 *Chem. Phys.*, 11, 10733-10741, doi:10.5194/acp-11-10733-2011, 2011.

700 Kinne, S., Schulz, M., Textor, C., Guibert, S., Balkanski, Y., Bauer, S. E., Berntsen, T., Berglen, T.
701 F., Boucher, O., Chin, M., Collins, W., Dentener, F., Diehl, T., Easter, R., Feichter, J., Fillmore,
702 D., Ghan, S., Ginoux, P., Gong, S., Grini, A., Hendricks, J., Herzog, M., Horowitz, L., Isaksen,
703 I., Iversen, T., Kirkevåg, A., Kloster, S., Koch, D., Kristjansson, J. E., Krol, M., Lauer, A.,
704 Lamarque, J. F., Lesins, G., Liu, X., Lohmann, U., Montanaro, V., Myhre, G., Penner, J., Pitari,
705 G., Reddy, S., Seland, O., Stier, P., Takemura, T., and Tie, X.: An AeroCom initial assessment –
706 optical properties in aerosol component modules of global models, *Atmos. Chem. Phys.*, 6,
707 1815-1834, doi:10.5194/acp-6-1815-2006, 2006.

708 Lafon, S., Rajot, J.-L., Alfaro, S. C., and Gaudichet, A.: Quantification of iron oxides in desert
709 aerosol, *Atmos. Environ.*, 38, 1211-1218, 2004.

710 Lafon, S., Sokolik, I. N., Rajot, J. L., Caquineau, S., and Guadichet, A.: Characterization of iron
711 oxides in mineral dust aerosols: Implications for light absorption, *J. Geophys. Res.*, 111,
712 D21207, doi:10.1029/2005JD007016, 2006.



713 Li, Z., Li, C., Chen, H., Tsay, S.-C., Holben, B., Huang, J., Li, B., Maring, H., Qian, Y., Shi, G.,
714 Xia, X., Yin, Y., Zheng, Y., and Zhuang, G.: East Asian Studies of Tropospheric Aerosols and
715 their Impact on Regional Climate (EAST-AIRC): An overview, *J. Geophys. Res.*, 116, D00K34,
716 doi:10.1029/2010JD015257, 2011.

717 Mikami, M., Shi, G. Y., Uno, I., Yabuki, S., Iwasaka, Y., Yasui, M., Aoki, T., Tanaka, T. Y.,
718 Kuroasaki, Y., Masuda, K., Uchiyama, A., Matsuki, A., Sakai, T., Takemi, T., Nakawo, M., Seino,
719 N., Ishizuka, M., Satake, S., Fujita, K., Hara, Y., Kai, K., Kanayama, S., Hayashi, M., Du, M.,
720 Kanai, Y., Yamada, Y., Zhang, X. Y., Shen, Z., Zhou, H., Abe, Q., Nagai, T., Tsutsumi, Y., Chiba,
721 M., and Suzuki, J.: Aeolian dust experiment on climate impact: An overview of Japan-China
722 joint project ADEC, *Global Planet. Change*, 52, 142-172, doi:10.1016/j.gloplacha.2006.03.001,
723 2006.

724 Morman, S. A. and Plumlee, G. S.: The role of airborne mineral dusts in human disease, *Aeolian*
725 *Res.*, 9, 203-212, 2013.

726 Nakajima, T., Tonna, G., Rao, R., Boi, P., Kaufman, Y., and Holben, B.: Use of sky brightness
727 measurements from ground for remote sensing of particulate polydispersions, *Appl. Opt.*,
728 35(15), 2672-2686, doi:10.1364/AO.35.002672, 1996.

729 Nakajima, T., Sekiguchi, M., Takemura, T., Uno, I., Higurashi, A., Kim, D., Sohn, B. J., Oh, S. -N.,
730 Nakajima, T. Y., Ohta, S., Okada, I., Takamura, T., and Kawamoto, K.: Significance of direct and
731 indirect radiative forcings of aerosols in the East China Sea region, *J. Geophys. Res.*, 108(D23),
732 8658, doi:10.1029/2002JD003261, 2003.

733 Okin, G. S., Mahowald, N., Chadwick, O. A., and Artaxo, P.: Impact of desert dust on the
734 biogeochemistry of phosphorus in terrestrial ecosystems, *Global Biogeochem. Cycles*, 18,
735 GB2005, doi:10.1029/2003GB002145, 2004.

736 Pandithurai, G., Dipu, S., Dani, K. K., Tiwari, S., Bisht, D. S., Devara, P. C. S., and Pinker, R. T.:
737 Aerosol radiative forcing during dust events over New Delhi, India, *J. Geophys. Res.*, 113,
738 D13209, doi:10.1029/2008JD009804, 2008.

739 Patterson, E. M., Gillette, D. A., and Stockton, B.: Complex index of refraction between 300 and
740 700 nm for Saharan aerosols, *J. Geophys. Res.*, 82(21), 3153-3160, 1977.

741 Perlitz, J., Tegen, I., and Miller, R. L.: Interactive soil dust aerosol model in GISS GCM, 1.
742 Sensitivity of the soil dust cycle to radiative properties of soil dust aerosols, *J. Geophys. Res.*,



743 106, D16, 18167-18192, 2001.

744 Prospero, J. M., Ginoux, P., Torres, O., Nicholson, S. E., and Gill, T. E.: Environmental
745 characterization of global sources of atmospheric soil dust identified with the Nimbus 7 total
746 ozone mapping spectrometer (TOMS) absorbing aerosol product, *Rev. Geophys.*, 40(1), 1002,
747 doi:10.1029/2000RG000095, 2002.

748 Ramanathan, V., Crutzen, P. J., Kiehl, J. T., and Rosenfeld, D.: Aerosols, climate, and the
749 hydrological cycle, *Science*, 294, 2119-2124, doi:10.1126/science.1064034, 2001.

750 Ricchiazzi, P., Yang, S., Gautier, C., and Sowle, D.: SBDART: A research and teaching software
751 tool for plane-parallel radiative transfer in the Earth's atmosphere, *Bull. Amer. Meteor. Soc.*, 79,
752 2101-2114, 1998.

753 Rosenfeld, D., Rudich, Y., and Lahav, R.: Desert dust suppressing precipitation: A possible
754 desertification feedback loop, *Proc. Natl. Acad. Sci. U.S.A.*, 98, 5975-5980, 2001.

755 Shao, Y., Wyrwoll, K.-H., Chappel, A., Huang, J., Lin, Z., McTainsh, G., Mikami, M., Tanaka, T.,
756 Wang, X., and Yoon, S.: Dust cycle: An emerging core theme in Earth system science, *Aeolian*
757 *Res.*, 2, 181-204, 2011.

758 Shen, Z., Sun, J., Cao, J., Zhang, L., Zhang, Q., Lei, Y., Gao, J., Huang, R., Liu, S., Huang, Y.,
759 Zhu, C., Xu, H., Zheng, C., Liu, P., and Xue, Z.: Chemical profiles of urban fugitive dust PM2.5
760 samples in Northern Chinese cities, *Sci. Total Environ.*, 569-570, 619-626,
761 doi:10.1016/j.scitotenv.2016.06.156, 2016.

762 Smirnov, A., Holben, B. N., Eck, T. F., Dubovik, O., and Slutsker, I.: Cloud screening and quality
763 control algorithms for the AERONET database, *Remote Sens. Environ.*, 73, 337-349, 2000.

764 Smirnov, A., Holben, B. N., Kaufman, Y. J., Dubovik, O., Eck, T. F., Slutsker, I., Pietras, C., and
765 Halthore, R.: Optical properties of atmospheric aerosol in maritime environments, *J. Atmos.*
766 *Sci.*, 59, 501-523, 2002.

767 Sokolik, I. N. and Golitsyn, G.: Investigation of optical and radiative properties of atmospheric
768 dust aerosols, *Atmos. Environ.*, 27A, 16, 2509-2517, 1993.

769 Sokolik, I. N. and Toon, O. B.: Incorporation of mineralogical composition into models of the
770 radiative properties of mineral aerosol from UV to IR wavelengths, *J. Geophys. Res.*, 104, D8,
771 9423-9444, 1999.

772 Sokolik, I. N., Winker, D. M., Bergametti, G., Gillette, D. A., Garmichael, G., Kaufman, Y. J.,



773 Gomes, L., Schuetz, L., and Penner, J. E.: Introduction to special section: Outstanding problems
774 in quantifying the radiative impacts of mineral dust, *J. Geophys. Res.*, 106, D16, 18015-18027,
775 2001.

776 Takamura, T., Nakajima, T., and SKYNET community group: Overview of SKYNET and its
777 Activities, *Opt. Puray Apl.*, 37, 3303-3308, 2004.

778 Tegen, I. and Fung, I.: Contribution to the atmospheric mineral aerosol load from land surface
779 modification, *J. Geophys. Res.*, 100, 18707-18726, doi:10.1029/95JD02051, 1995.

780 Todd, M. C., Washington, R., Martins, J. V., Dubovik, O., Lizcano, G., M'Bainayel, S., and
781 Engelstaedter, S.: Mineral dust emission from the Bodélé Depression, northern Chad, during
782 BoDEX 2005, *J. Geophys. Res.*, 112, D06207, doi:10.1029/2006JD007170, 2007.

783 Uchiyama, A., Yamazaki, A., Togawa, H., Asano, J., and Shi, G.-Y.: Single scattering albedo of
784 Aeolian dust as inferred from sky-radiometer and in situ ground-based measurement, SOLA,
785 Vol. 1, pp. 209-212, doi:10.2151/sola.2005-054, 2005.

786 Uno, I., Eguchi, K., Yumimoto, K., Takemura, T., Shimizu, A., Uematsu, M., Liu, Z., Wang, Z.,
787 Hara, Y., and Sugimoto, N.: Asian dust transported one full circuit around the globe, *Nature
788 Geosci.*, 2, 557-560, doi:10.1038/NGEO583, 2009.

789 Uno, I., Eguchi, K., Yumimoto, K., Liu, Z., Hara, Y., Sugimoto, N., Shimizu, A., and Takemura, T.:
790 Large Asian dust layers continuously reached North America in April 2010, *Atmos. Chem.
791 Phys.*, 11, 7333-7341, 2011.

792 Wang, G., Huang, J., Guo, W., Zuo, J., Wang, J., Bi, J., Huang, Z., and Shi, J.: Observation
793 analysis of land-atmosphere interactions over the Loess Plateau of northwest China, *J. Geophys.
794 Res.*, 115, D00K17, doi:10.1029/2009JD013372, 2010a.

795 Wang, H., Shi, G. Y., Aoki, T., Wang, B., and Zhao, T. L.: Radiative forcing due to dust aerosol
796 over east Asia-north Pacific region during spring, 2001, *Chin. Sci. Bull.*, 49(20): 2212-2219,
797 2004.

798 Wang, H., Zhang, X., Gong, S., Chen, Y., Shi, G., and Li, W.: Radiative feedback of dust aerosols
799 on the East Asian dust storms, *J. Geophys. Res.*, 115, D23214, doi:10.1029/2009JD013430,
800 2010b.

801 Wang, W., Huang, J., Minnis, P., Hu, Y., Li, J., Huang, Z., Ayers, J. K., and Wang, T.: Dusty cloud
802 properties and radiative forcing over dust source and downwind regions derived from A-Train



803 data during the Pacific Dust Experiment, *J. Geophys. Res.*, 115, D00H35,
804 doi:10.1029/2010JD014109, 2010c.

805 Wang, X., Huang, J., Ji, M., and Higuchi, K.: Variability of East Asia dust events and their
806 long-term trend, *Atmos. Environ.*, 42, 13, 3156-3165, doi:10.1016/j.atmosenv.2007.07.046,
807 2008.

808 Wang, X., Doherty, S. J., and Huang, J.: Black carbon and other light-absorbing impurities in
809 snow across Northern China, *J. Geophys. Res.*, 118, 1471-1492, doi:10.1029/2012JD018291,
810 2013.

811 Wang, X., Pu, W., Shi, J., Bi, J., Zhou, T., Zhang, X., and Ren, Y.: A comparison of the physical
812 and optical properties of anthropogenic air pollutants and mineral dust over Northwest China, *J.*
813 *Meteorol. Res.*, 29, 180-200, doi:10.1007/s13351-015-4092-0, 2015.

814 Wang, Y., Wang, R., Ming, J., Liu, G., Chen, T., Liu, X., Liu, H., Zhen, Y., and Cheng, G.: Effects
815 of dust storm events on weekly clinic visits related to pulmonary tuberculosis disease in Minqin,
816 China, *Atmos. Environ.*, 127, 205-212, 2016.

817 World Meteorological Organization (WMO), Report of the Experts Meeting on Aerosols and Their
818 Climatic Effects, WCP-55, Geneva, Switzerland, 1983.

819 Wu, F., D. Zhang, J. Cao, H. Xu, and Z. An: Soil-derived sulfate in atmospheric dust particles at
820 Taklimakan desert, *Geophys. Res. Lett.*, 39, L24803, doi:10.1029/2012GL054406, 2012.

821 Wu, F., D. Zhang, J. Cao, T. Zhang, and Z. An: Background-like nitrate in desert air, *Atmos.*
822 *Environ.*, 84, 39-43, 2014.

823 Xia, X., Chen, H., Goloub, P., Zhang, W., Chatenet, B., and Wang, P.: A compilation of aerosol
824 optical properties and calculation of direct radiative forcing over an urban region in northern
825 China, *J. Geophys. Res.*, 112, D12203, doi:10.1029/2006JD008119, 2007.

826 Xu, J., Bergin, M. H., Greenwald, R., Schauer, J. J., Shafer, M. M., Jaffrezo, J. L., and Aymoz, G.:
827 Aerosol chemical, physical, and radiative characteristics near a desert source region of
828 northwest China during ACE-Asia, *J. Geophys. Res.*, 109, D19S03, doi:10.1029/2003JD004239,
829 2004.

830 Yang, M., Howell, S. G., Zhuang, J., and Huebert, B. J.: Attribution of aerosol light absorption to
831 black carbon, brown carbon, and dust in China—interpretations of atmospheric measurements
832 during EAST-AIRE, *Atmos. Chem. Phys.*, 9, 2035-2050, doi:10.5194/acp-9-2035-2009, 2009.



833 Zhang, X., Arimoto, R., and An, Z.: Dust emission from Chinese desert sources linked to
834 variations in atmospheric circulation, *J. Geophys. Res.*, 102, D23, 28041-28047,
835 doi:10.1029/97JD02300, 1997.

836

837

838

839

840

841

842

843

844

845

846

847

848

849

850

851

852

853

854

855

856

857

858

859

860

861

862



863 **Figure captions**

864

865 **Table 1.** Overall average and standard deviation of key optical properties at 550 nm (e.g.,
 866 single-scattering albedo, asymmetry factor, real part and imaginary part of complex refractive
 867 index) for Asian pure Dust (PDU). Ångström wavelength exponent (α) is in the range of 440-870
 868 nm. Minimum and maximum values of the optical properties are in parenthesis for each
 869 corresponding column. Measuring period and the total number of PDU ($\alpha < 0.2$) and Transported
 870 Anthropogenic Dust (TDU, $0.2 < \alpha < 0.6$) days are in the parenthesis for the first and last column,
 871 respectively.

872

Site (sampled period)	SSA (min, max)	ASY (min, max)	Re (min, max)	Ri ($\times 10^{-3}$)	Ångström (440-870 nm)	PDU/days (TDU)
SACOL (2006-2012)	0.932 \pm 0.018 (0.888, 0.971)	0.741 \pm 0.012 (0.715, 0.771)	1.534 \pm 0.044 (1.438, 1.60)	2.251 \pm 0.788 (0.913, 5.51)	0.120 \pm 0.049 (0.0, 0.198)	38 (97)
Dalanzadgad (1997-2014)	0.930 \pm 0.012 (0.912, 0.949)	0.746 \pm 0.010 (0.724, 0.766)	1.512 \pm 0.046 (1.447, 1.60)	2.407 \pm 0.414 (1.649, 3.19)	0.127 \pm 0.079 (-0.06, 0.199)	8 (6)
Beijing (2001-2015)	0.917 \pm 0.020 (0.863, 0.963)	0.742 \pm 0.012 (0.716, 0.769)	1.557 \pm 0.043 (1.401, 1.60)	2.801 \pm 0.865 (1.032, 6.20)	0.117 \pm 0.067 (-0.048, 0.199)	46 (67)
Yulin (2001-2002)	0.907 \pm 0.024 (0.863, 0.952)	0.748 \pm 0.010 (0.731, 0.771)	1.559 \pm 0.038 (1.476, 1.60)	3.564 \pm 1.589 (1.370, 7.92)	0.077 \pm 0.068 (-0.024, 0.188)	13 (16)
Dushanbe (2010-2015)	0.941 \pm 0.012 (0.916, 0.959)	0.739 \pm 0.011 (0.710, 0.765)	1.529 \pm 0.041 (1.436, 1.60)	2.011 \pm 0.551 (1.022, 3.475)	0.128 \pm 0.054 (-0.02, 0.198)	26 (95)
Karachi (2006-2014)	0.945 \pm 0.012 (0.916, 0.977)	0.741 \pm 0.011 (0.714, 0.767)	1.518 \pm 0.030 (1.449, 1.60)	1.938 \pm 0.561 (0.758, 3.439)	0.141 \pm 0.041 (-0.005, 0.20)	83 (286)
Lahore (2007-2015)	0.930 \pm 0.014 (0.901, 0.957)	0.740 \pm 0.010 (0.721, 0.765)	1.519 \pm 0.038 (1.432, 1.60)	2.253 \pm 0.611 (1.207, 3.623)	0.136 \pm 0.052 (0.023, 0.198)	26 (248)
IASBS (2010-2013)	0.933 \pm 0.017 (0.883, 0.958)	0.725 \pm 0.011 (0.704, 0.746)	1.572 \pm 0.024 (1.525, 1.60)	2.290 \pm 0.845 (1.245, 5.029)	0.098 \pm 0.050 (0.021, 0.195)	19 (12)
Kandahar (2008/04-06)	0.925 \pm 0.013 (0.903, 0.955)	0.729 \pm 0.017 (0.700, 0.768)	1.534 \pm 0.035 (1.492, 1.60)	2.855 \pm 0.775 (1.445, 4.65)	0.147 \pm 0.054 (0.00, 0.199)	10 (4)
Dunhuang (2001/03-05)	0.947 \pm 0.015 (0.918, 0.970)	0.745 \pm 0.013 (0.723, 0.761)	1.547 \pm 0.037 (1.494, 1.60)	1.714 \pm 0.697 (1.014, 3.14)	0.039 \pm 0.029 (-0.003, 0.091)	6 (0)
Dunhuang_LZU (2012/04-05)	0.958 \pm 0.007 (0.951, 0.968)	0.741 \pm 0.021 (0.707, 0.771)	1.495 \pm 0.042 (1.451, 1.580)	1.589 \pm 0.292 (1.092, 1.84)	0.153 \pm 0.026 (0.117, 0.184)	5 (4)
Inner_Mongolia (2001/04-05)	0.948 \pm 0.012 (0.930, 0.960)	0.751 \pm 0.006 (0.743, 0.759)	1.499 \pm 0.042 (1.426, 1.54)	1.641 \pm 0.457 (1.169, 2.45)	0.069 \pm 0.054 (0.011, 0.165)	4 (1)
Minqin (2010/05-06)	0.945 \pm 0.002 (0.942, 0.947)	0.756 \pm 0.014 (0.740, 0.764)	1.469 \pm 0.023 (1.449, 1.494)	2.036 \pm 0.220 (1.883, 2.29)	0.119 \pm 0.023 (0.103, 0.146)	2 (0)
Overall Mean	0.935\pm0.014	0.742\pm0.008	1.526\pm0.029	2.258\pm0.556	0.113\pm0.033	PDU
Overall Mean	0.921\pm0.021	0.723\pm0.009	1.521\pm0.025	3.643\pm1.372	0.355\pm0.06	TDU

873

874



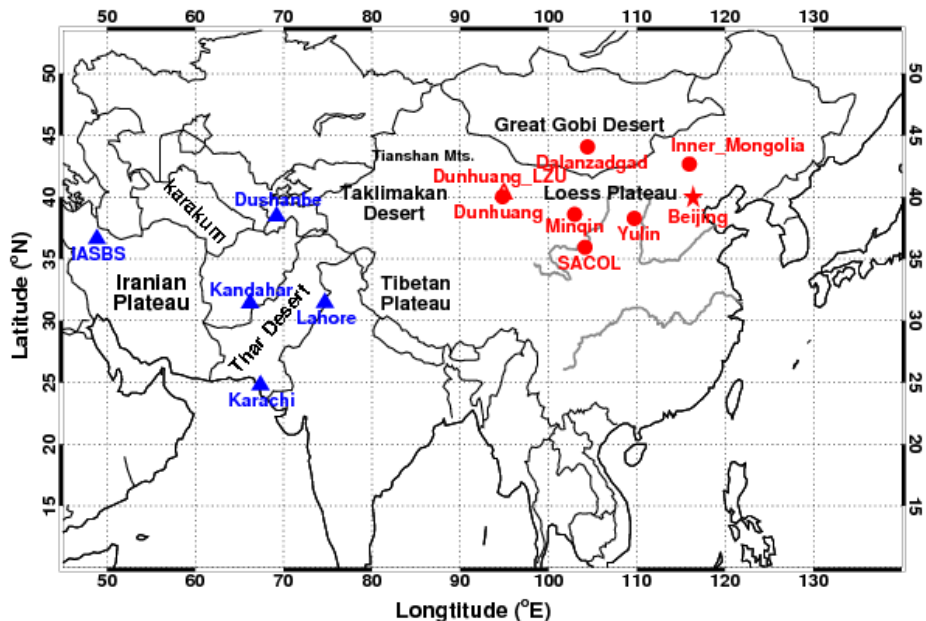
875

876 **Table 2.** Spectral optical properties of Pure Dust ($\alpha < 0.2$) and Transported Anthropogenic Dust
 877 ($0.2 < \alpha < 0.6$) averaged for 13 sites over East and Central Asia areas.

Asian Dust	Pure Dust ($\alpha < 0.2$)	Transported Anthropogenic Dust ($0.2 < \alpha < 0.6$)
$\omega_0(440/675/870/1020)$	0.906/0.962/0.971/0.975 ± 0.009	0.897/0.943/0.954/0.959 ± 0.019
$Re(440/675/870/1020)$	1.520/1.533/1.517/1.503 ± 0.026	1.509/1.533/1.532/1.525 ± 0.027
$Ri(440/675/870/1020) \times 10^{-3}$	3.413/1.574/1.449/1.449 ± 0.450	5.064/2.737/2.510/2.486 ± 1.300
$ASY(440/675/870/1020)$	0.758/0.727/0.724/0.726 ± 0.008	0.736/0.711/0.710/0.712 ± 0.009
r_{Vf} (μm); σ_f	0.159 ± 0.029	0.140 ± 0.011
r_{Vc} (μm); σ_c	2.157 ± 0.112	2.267 ± 0.214
Cvf ($\mu\text{m}^3/\mu\text{m}^2$)	0.037 ± 0.011 ; $0.06 \times \tau(1020) - 0.001$	0.038 ± 0.011 ; $0.12 \times \tau(1020) - 0.014$
Cvc ($\mu\text{m}^3/\mu\text{m}^2$)	0.632 ± 0.167 ; $0.88 \times \tau(1020) - 0.07$	0.343 ± 0.084 ; $0.90 \times \tau(1020) - 0.06$
Cvc/Cvf	17.9 (11~31)	9.1 (5~11)

878 Each variable is accompanied by a standard deviation (e.g., ± 0.01). r_{Vf} and r_{Vc} are the volume
 879 median radii of fine-mode and coarse-mode particles in μm ; Cvf and Cvc denote the volume
 880 concentrations of fine-mode and coarse-mode particles in $\mu\text{m}^3/\mu\text{m}^2$, respectively. The dynamic
 881 dependencies of dust optical properties are exhibited as functions of AOD_{1020} , with correlation
 882 coefficients greater than 0.93 for all cases.

883



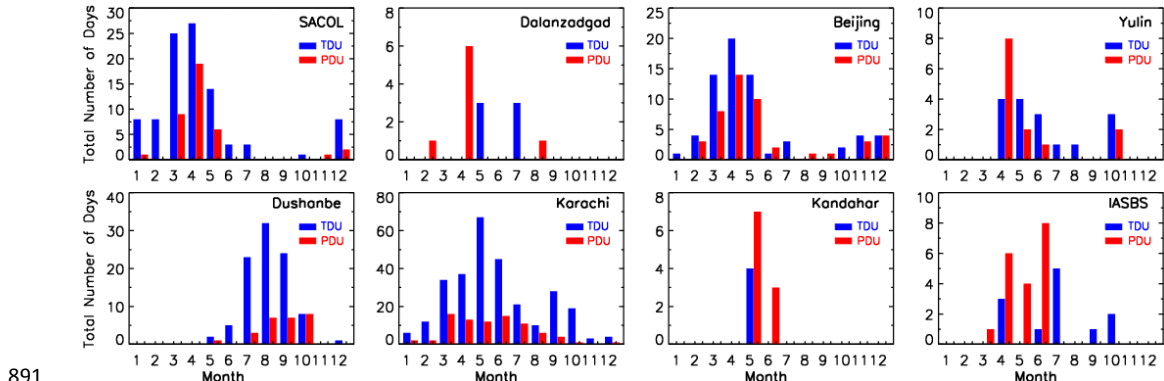
884

885 **Figure 1.** Geographical location of selected 13 AERONET sites in this study. Eight sites over East
 886 Asian region are labeled with red colors, and five sites over Central Asian region are labeled with
 887 blue colors. The major Great deserts or Gobi deserts along with plateaus are marked with black
 888 font.

889



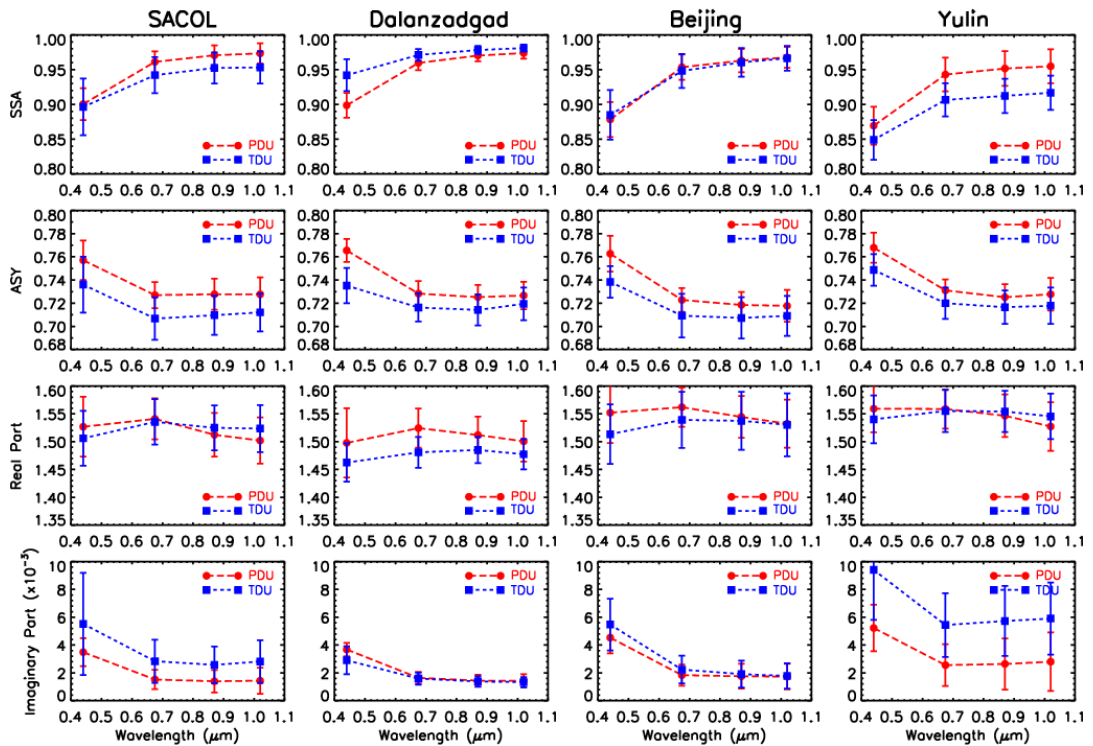
890



891

892 **Figure 2.** Occurrence frequency of total number days for Pure Dust ($\alpha < 0.2$, PDU with red color)
 893 and Transported Anthropogenic Dust ($0.2 < \alpha < 0.6$, TDU with blue color) at selected four East
 894 Asian sites (top panel) and four Central Asian sites (bottom panel).

895

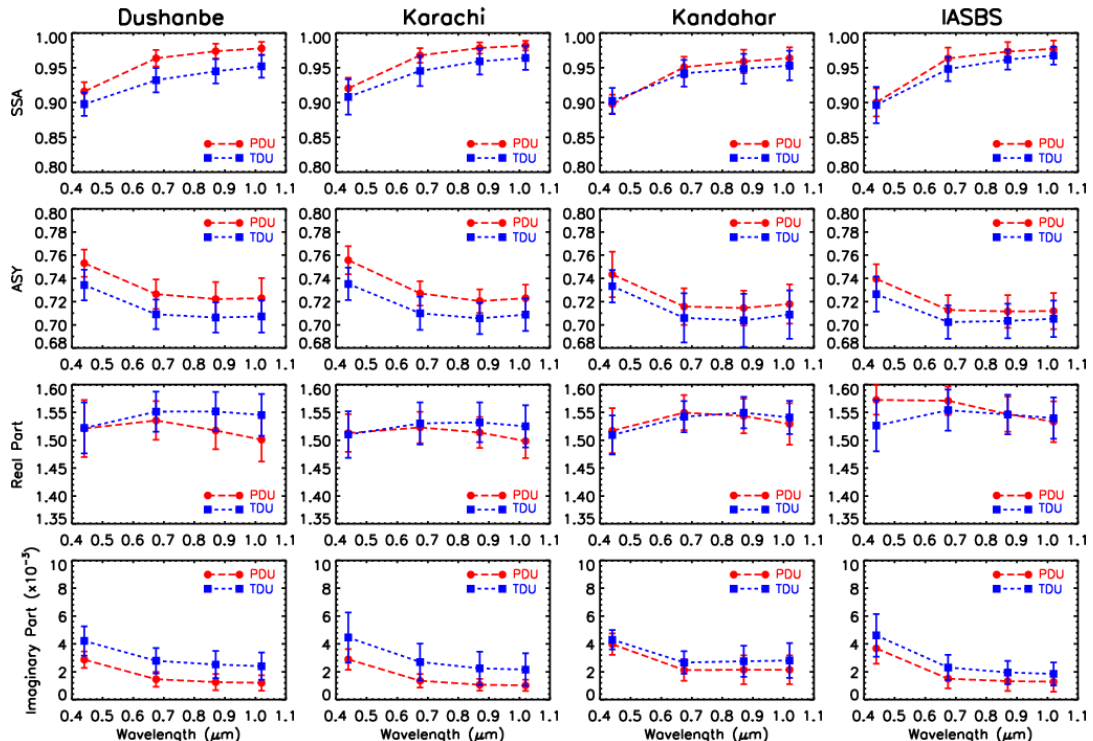


896

897 **Figure 3.** Overall average spectral behavior of key optical properties for Pure Dust ($\alpha < 0.2$, PDU
 898 with red circle) and Transported Anthropogenic Dust ($0.2 < \alpha < 0.6$, TDU with blue square) at
 899 selected four East Asian sites (SACOL, Dalanzadgad, Beijing and Yulin). The error bars indicate
 900 plus or minus one standard deviation.



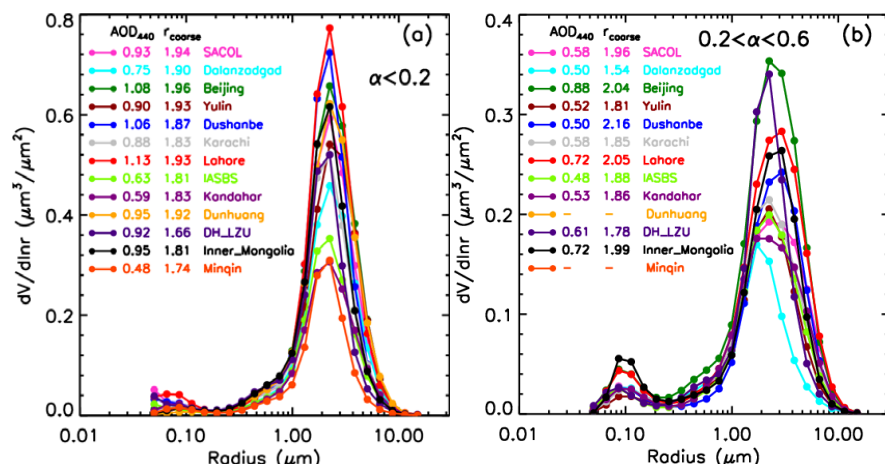
901



902

903 **Figure 4.** The same as Figure 3, but for selected four Central Asian sites (Dushanbe, Karachi,
 904 Kandahar and IASBS).

905



906
 907 **Figure 5.** Overall average of aerosol volume size distributions in the entire atmospheric column
 908 for (a) Pure Dust ($\alpha < 0.2$) and (b) Transported Anthropogenic Dust ($0.2 < \alpha < 0.6$) at selected 13
 909 AERONET sites. Corresponding aerosol optical depth at 440 nm (AOD_{440}) and effective radius of



910 coarse mode (r_{coarse}) in μm are also shown.

911

912

913

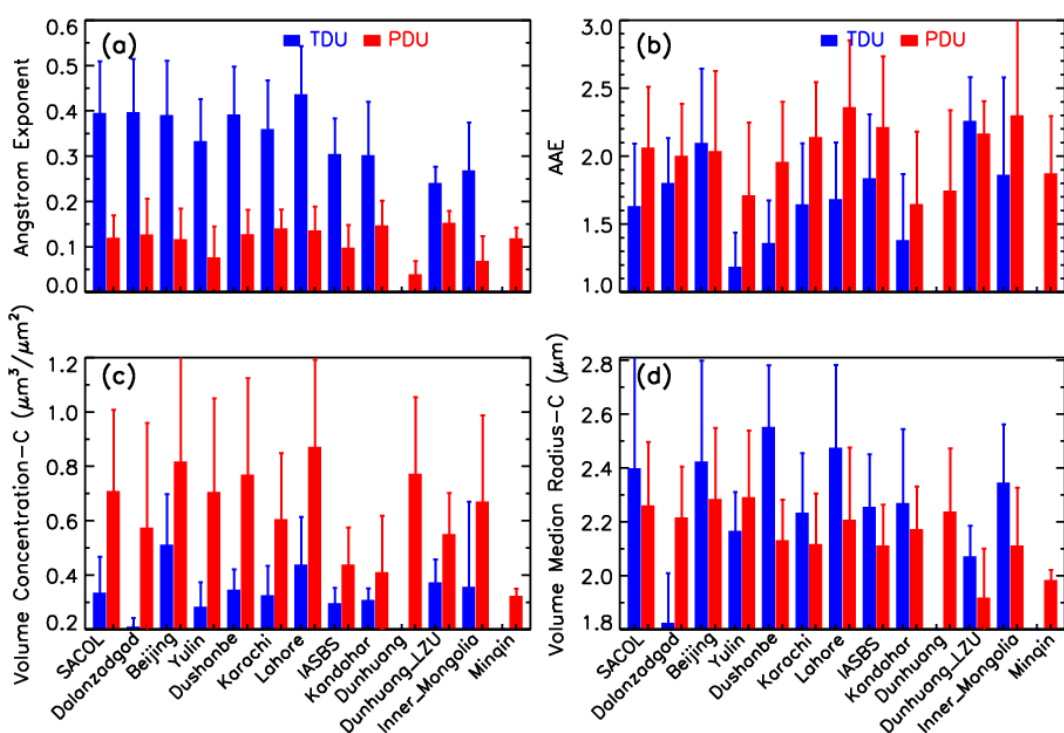
914

915

916

917

918



919

920 **Figure 6.** Total average values of (a) Ångström exponent (440-870 nm), (b) absorption Ångström
 921 exponent at 440-870 nm (AAE), (c) volume concentration of coarse mode ($\mu\text{m}^3/\mu\text{m}^2$), and (d)
 922 volume median radius of coarse mode in μm for Transported Anthropogenic Dust ($0.2 < \alpha < 0.6$,
 923 blue color) and Pure Dust ($\alpha < 0.2$, red color) at 13 selected AERONET sites. The error bars
 924 indicate plus or minus one standard deviation.

925

926

927

928

929

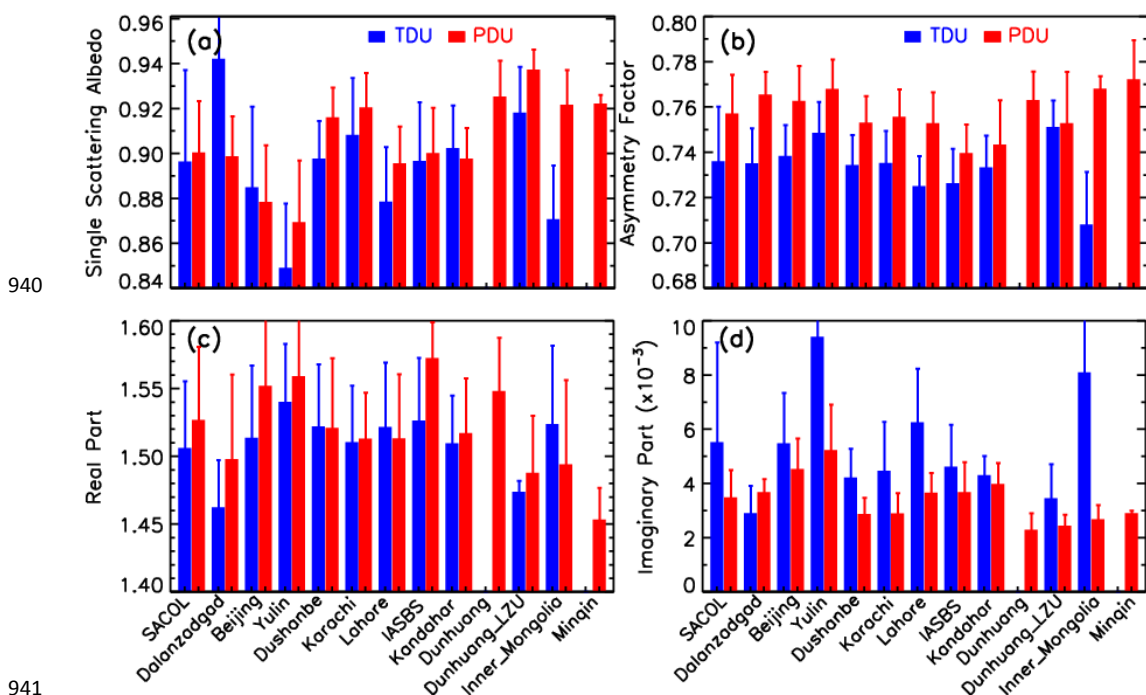
930

931

932



933
934
935
936
937
938
939

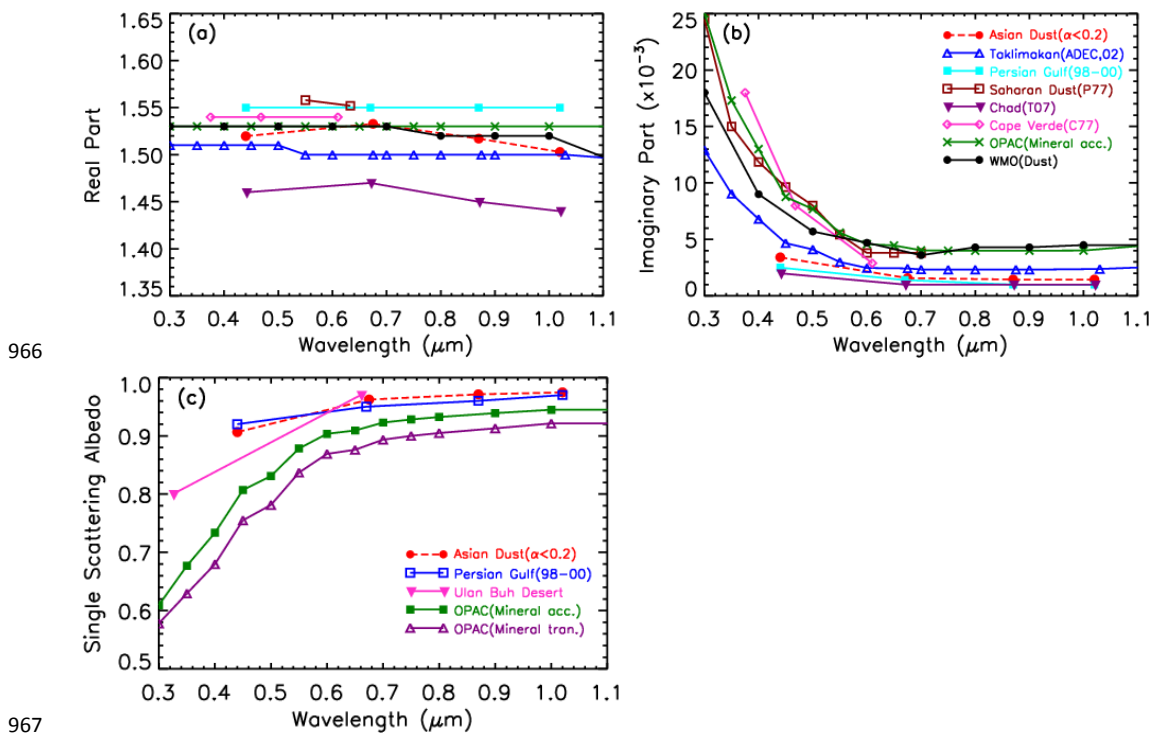


940
941
942 **Figure 7.** The same as Figure 5, but for (a) sing-scattering albedo, (b) asymmetry factor, (c) real
943 part and (d) imaginary part of complex refractive index at 440 nm.

944
945
946
947
948
949
950
951
952
953
954
955
956
957



958
 959
 960
 961
 962
 963
 964
 965

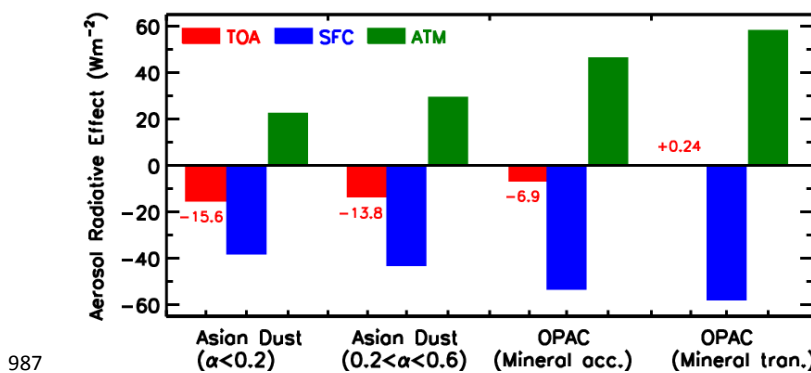


966
 967
 968
 969
 970
 971
 972
 973
 974
 975
 976
 977
 978
 979
 980
 981

Figure 8. Mean spectral behaviors of (a) real part, (b) imaginary part of complex refractive index, and (c) single-scattering albedo for Asian Pure Dust ($\alpha < 0.2$) calculated for 13 AERONET sites, and results of current common dust models (OPAC, WMO), Bahrain-Persian Gulf of Desert dust (1998-2000), Saharan dust (Chad, Cape Verde Islands), and Chinese Gobi desert (Taklimakan, Ulan Buh Desert) are also shown for comparison.



982
983
984
985
986



987
988 **Figure 9.** Aerosol shortwave direct radiative effects at the top of the atmosphere (TOA, red color),
989 at the surface (SFC, blue color), and in the atmospheric layer (ATM, green color) for Asian Pure
990 Dust ($\alpha < 0.2$) and Transported Anthropogenic Dust ($0.2 < \alpha < 0.6$) computed in this study, and
991 corresponding values for OPAC Mineral accumulated (Mineral acc.) and transported (Mineral
992 tran.) modes are also presented for comparison.

993